Thermalization related effects in the electrofission of preactinide nuclei

J. D. T. Arruda-Neto,* T. Saito, M. Sugawara, T. Tamae, H. Miyase, K. Abe, K. Takahisa, O. Konno, and M. Oikawa
Laboratory of Nuclear Science, Tohoku University, Sendai, Japan

A. Deppman and S. Simionatto
Physics Institute, University of Saõ Paulo, Saõ Paulo, Brazil
(Received 25 October 1993)

The absolute electrofission cross section of Au and Ta was measured in the energy interval 40–250 MeV. Pronounced inflexions of the (e,f) curves are observed for both Au and Ta around 200–220 MeV, which are signatures of structures in the corresponding photofission cross-section curves. We show that these (γ,f) structures are originated in the stage of preequilibrium emissions in the nuclear thermalization process. The question associated to a possible connection between thermalization effects and competing photoexcitation mechanisms is addressed.

PACS number(s): 24.75.+i, 25.85.Jg, 25.85.Ge, 27.80.+w

I. INTRODUCTION

Photonuclear reactions (induced by real or virtual photons) are very suitable to probe the nuclear and nucleonic structure, for the reaction mechanism is well understood comparative to the nucleon-nucleon interactions.

For photon energies above the photopion production threshold ($\sim$ 140 MeV), in particular, pion production is the dominant process responsible for photoabsorption. At these energies, the absorption of a photon initiates an intranuclear cascade (the fast step, with a duration $\tau_0 < 10^{-22}$ s) in which particles of the continuum leave the nucleus (preequilibrium emission) all along until equilibration (compound nucleus formation); as pointed out before [1,2], in this system the thermodynamic equilibrium is reached very quickly, during a time $\tau_{eq} > (5\text{–}10)\tau_0$. In the second step (the slow step) the compound nucleus evaporates particles or goes into fission.

It is a well-known fact that fission is a slow process ($\tau_f \sim 10^{-19}$ s) which occurs from an equilibrated nuclear system; this makes fission particularly valuable for studies of the target residues remaining after the preequilibrium emissions. Well known also is the use of fission as a filter for studying reactions mechanisms (as recently reviewed by Viola [3])—in this paper we explore such a possibility.

In this regard, electro- and photofission of preactinide nuclei are very convenient because of the following reasons: (1) As mentioned above, the primary process (photoexcitation) is well understood; (2) the photon can transfer substantial amounts of energy to the nucleus, but with comparatively small transfer of linear and angular momenta, which allows the observation of excitation energy effects *alone* (as evidenced in this work); (3) as nuclear matter is very transparent to photons, the whole nuclear volume is probed in a photoexcitation process. For example, pion photoproduction would occur, in principle, with equal probability in all nucleons of the nucleus, with these nucleons acting as pion radiators. (4) Different from what is verified for actinide (where fission barriers are $\sim$ 6 MeV), the fissility of preactinides (where fission barriers are of the order of 20–30 MeV) is a strong function of the excitation energy, which, by its turn, reflects peculiarities of the nuclear thermalization process (details below).

The electrofission of the preactinide nuclei ^{208}Pb and ^{209}Bi has been recently investigated in our laboratory [4,5]. A clear inflexion for ^{208}Pb, and a less pronounced one for ^{209}Bi, were observed in the electrofission cross-section curves around 200–220 MeV. These findings were tentatively interpreted as being due to the behavior of the photopions inside the nucleus as revealed by their mean free path. Although appealing, the results for ^{208}Pb and ^{209}Bi call for more experiments and, particularly, with emphasis in the energy region around 200–220 MeV.

Recently, Lucherini *et al.* [6] measured in Frascati the photofission cross section of Au with quasimonochromatic photons, in the energy range of 120–300 MeV. Because of the quasimonochromatic nature of the photons, a photofission yield curve (integrated over the photon spectra) is obtained. It is interesting to note that this photofission yield exhibits two clear inflexions around 150 and 190 MeV (see Fig. 1), and a third one, with less statistical significance, around 230 MeV. It is worth remembering that Fig. 1 (adapted from Ref. [6]) shows the Au(γ,f) *integral* yield, before deconvolution (we discuss this issue in Sec. IV B).

In this paper we present results for the electrofission cross section of the preactinides Au and Ta; the energy region around the supposed inflexions ($\sim$ 200–220 MeV) was carefully measured at intervals of 5 MeV. A simple visual inspection of the cross-section curves, for both Au and Ta, reveals the presence of inflexions similar to those observed for ^{208}Pb and ^{209}Bi. By means of an

*Permanent address: Physics Institute, University of Saõ Paulo, Saõ Paulo, Brazil.

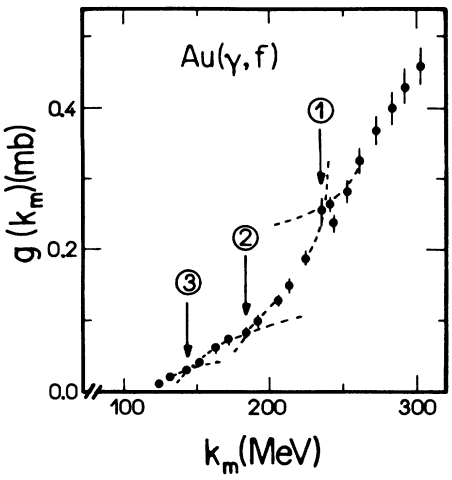

FIG. 1. Au photofission yield per equivalent quantum vs the maximum photon energy k_m, measured at Frascati (adapted from Ref. [6]). We added dashed lines to guide the eyes and numbered arrows to indicate the inflexions (details in the text).

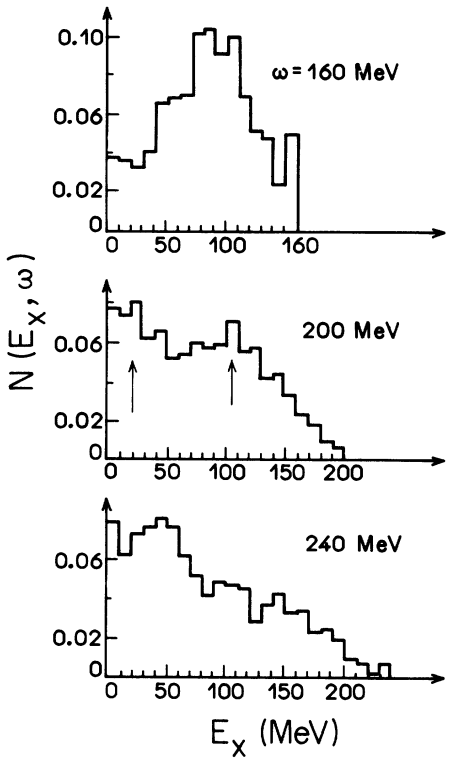

FIG. 2. E_x distribution functions $N(E_x,\omega)$ of the compound nuclei produced in the photoexcitation of Au, for ω = 160, 200, and 240 MeV. All histograms refer to Monte Carlo intranuclear-cascade calculations, from Refs. [7] and [8].

original data analysis and interpretation, we show, for the first time, that these inflexions are related to the nuclear thermalization process at its stage of preequilibrium emissions.

II. THEORETICAL ASPECTS

Structures in the photofission cross section $\sigma_{\gamma,f}$ manifest themselves as inflexions in the corresponding electrofission cross-section curve $\sigma_{e,f} = \sigma_{e,f}(E_e)$ because, by the virtual-photon theory,

$$\sigma_{e,f}(E_e) = \int_0^{E_e} \sigma_{\gamma,f}(\omega) N^{E1}(\omega, E_e) \frac{d\omega}{\omega}, \qquad (1)$$

where N^{E1} is the $E1$-virtual-photon spectrum, ω is the real (or virtual) photon energy, and E_e is the incident electron energy. We justify below why only the $E1$-virtual-photon spectrum is considered.

As discussed in the Introduction, the photofission of heavy nuclei following absorption of intermediate energy photons proceeds by means of a two-step process, where a compound nucleus $(A_{\rm CN}, Z_{\rm CN})$ with excitation energy E_x undergoes fission. However, for a given photon energy ω, E_x exhibits a distribution in the interval 0–ω (see Fig. 2); thus, we propose to express the (γ, f) cross section, related to a specific compound nucleus, as

$$\sigma_{\gamma,f}(A_{\rm CN}, Z_{\rm CN}; \omega) = \sum_i N(E_{x_i}, \omega) \sigma_{\rm CN}(A_{\rm CN}, Z_{\rm CN}; E_{x_i}, \omega) P_f(A_{\rm CN}, Z_{\rm CN}; E_{x_i}), \qquad (2)$$

where P_f is the fission probability, $\sigma_{\rm CN}$ is the cross section for compound nucleus formation, and $N(E_x,\omega)$ is the probability of finding a compound nucleus with excitation energy equal to E_x. In this regard, Guaraldo and collaborators [7,8] performed detailed calculations based on the intranuclear cascade model (as described in Ref. [7]) and obtained E_x distributions $N(E_x,\omega)$ in several nuclei, for photon energies between 100 and 300 MeV—these distributions are represented by histograms centered at E_{x_i} (Fig. 2). Then, the sum in Eq. (2) runs for all the histograms comprised in the energy interval 0–ω.

Since, in principle, several compound nuclei could be formed after the preequilibrium emissions, the experimentally obtained photofission cross section is given by

$$\sigma_{\gamma,f}(\omega) = \sum_{A_{\rm CN}, Z_{\rm CN}} \sigma_{\gamma,f}(A_{\rm CN}, Z_{\rm CN}; \omega). \qquad (3)$$

In the photon energy range pertinent to this paper, the $A_{\rm CN}$ and $Z_{\rm CN}$ distributions are not broad. In fact, at ω = 220 MeV for ^{197}Au we have [7]

$$\Delta A_{\rm CN} = A_t - \bar{A}_{\rm CN} \cong 1.5, \qquad (4)$$

$$\Delta Z_{\rm CN} = Z_t - \bar{Z}_{\rm CN} \cong 0.5, \qquad (5)$$

where A_t and Z_t refer to the target nucleus. Thus, we can simplify our theoretical approach by assuming that *only one* compound nucleus $(\bar{A}_{\rm CN}, \bar{Z}_{\rm CN})$, a "mean compound nucleus," is formed.

Also, we note that $\sigma_{\gamma,f}(\omega)$, Eqs. (2) and (3), depends explicitly on $\sigma_{\rm CN}$, which is a quantity not available experimentally. So, it is necessary to express $\sigma_{\rm CN}$ in terms of a well-known quantity as, e.g., the photoabsorption cross section $\sigma_{\gamma,a}(\omega)$. This was achieved by adopting, to the photonuclear reactions, a formalism developed by Kikuchi and Kawai [9] plus our "mean compound nucleus" assumption (details on the calculations will be published soon [10]), resulting in the following relationship:

$$\frac{\sigma_{\rm CN}(E_x)}{E_x} = \frac{\sigma_{\gamma,a}(\omega)}{\omega}, \quad \text{with } E_x = E_x(\omega). \tag{6}$$

Substituting Eq. (6) in Eq. (2) we obtain

$$\sigma_{\gamma,f}(\omega) = \frac{\sigma_{\gamma,a}(\omega)}{\omega} \sum_i N(E_{x_i},\omega) E_{x_i} P_f(\bar{A}_{\rm CN}, \bar{Z}_{\rm CN}; E_{x_i}). \tag{7}$$

This last result contains all the required physical quantities necessary for the data interpretation in this work. We note in passing that at $\omega \lesssim 180$ MeV the E_x distributions are nearly symmetric; then, if we substitute E_x by $\bar{E}_x$ in Eq. (7),

$$\sigma_{\gamma,f}(\omega) \simeq \sigma_{\gamma,a}(\omega) \frac{\bar{E}_x}{\omega} \sum_i N(E_{x_i},\omega) P_f(E_{x_i}), \tag{8}$$

where $\bar{E}_x/\omega$ is approximately constant for $\omega \lesssim 180$ MeV [7]. Therefore, the "effective" (γ, f) fissility is proportional to some sort of mean weight of the compound nucleus fission probability, $\sum_i N(E_{x_i},\omega) P_f(E_{x_i})$.

Since at energies below the peak of the delta resonance ($\sim$ 300 MeV) $\sigma_{\gamma,a}$ is a structureless function of ω, it is quite obvious that possible structures in the (γ, f) cross section are generated by the "mean weighted P_f". However, the fission probability of a preactinide nucleus is a smooth and steep rising function (nearly exponential) of E_x (see Table VII-1 of Ref. [11]); thus, only "distortions" in the distributions $N(E_x,\omega)$ could explain a drastic change in the slope of the (γ, f) curve, as reported in the present work for Au and Ta.

Finally, we note that at lower energies ($\omega \lesssim 50$ MeV), $E_x \cong \omega$ and, since $\sum_i N = 1$, our derived expression for $\sigma_{\gamma,f}$ [Eq. (7)] becomes trivially $\sigma_{\gamma,f}(\omega) = \sigma_{\gamma,a}(\omega) P_f(\omega)$.

III. EXPERIMENT AND RESULTS

In view of the facts and reasonings cited above, we decided to perform a careful and detailed measurement of the electrofission cross section of Au and Ta. The difficulties associated with possible $(e, e'f)$ exclusive measurements of preactinide nuclei have been pointed out elsewhere [12]; typical single-armed fission cross sections range from 10^{-3} to 1 microbarn. If coincidence is imposed, the $(e, e'f)$ cross sections become several orders of magnitude lower than that of (e, f), which makes these experiments very time consuming.

Targets of Au and Ta with high purity were irradiated with electron beams from the Tohoku University linear accelerator, with energies from 40 to 250 MeV in steps of 5 and 10 MeV. Mica foils were used as fission fragment detectors, and the electron beam was monitored by means of a ferrite core monitor. Details about the procedures and experimental set up were published elsewhere [4].

In Fig. 3 is shown our electrofission for Au and Ta in the energy interval 180–250 MeV, which corresponds to the energy region where the searched out inflexions are located. The data points in the full range, 40–250 MeV, were used for a better delineation of the unfolded (γ, f) curve (details below).

We would like to stress the following points:

(1) The reproducibility of the (e, f) experimental points is around 5–10%, so that the inflexions exhibited in Fig. 3 are not artifacts of the experimental fluctuations.

(2) The (e, f) curves of preactinides are steep functions of the energy, which makes the presence of inflexions and shoulders much more evident. For actinides the situation is opposite, because their fissilities saturates (around 100%) for energies above 50 MeV; as a consequence, the (e, f) curves are very flat and, therefore, do not respond accordingly to changes in E_x.

(3) The remarkable similarity between the Au and Ta (e, f) curves demonstrates the physical significance of the inflexions. We would say that the independently obtained Au and Ta curves are "twin curves" in a normalized scale, despite the fact that their absolute values differ by nearly one order of magnitude. Therefore, each

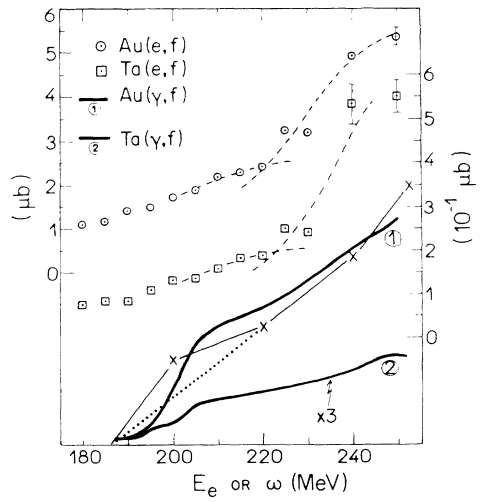

FIG. 3. Electrofission cross section of Au (left-hand scale) and Ta (right-hand scale); the dashed curves are to guide the eyes. The solid curves are the unfolded photofission cross sections of Au and Ta (in arbitrary unit)—the uncertainties, not shown, are $\sim$ 15%. The curves represented by ×—× and ··· are the calculated photofission cross section of Au (details in the text).

one of these nuclei works as a *veto* to the other. In this sense, an observed inflexion is accepted as a "physical fact" (and not a fluctuation) only if it is observed in *both nuclei* at the same energy position. The physical nature of the inflexions, shown in Fig. 3, is considerably reinforced by the occurrence of similar inflexions in ^{209}Bi and ^{208}Pb (see Fig. 3 of Ref. [5]).

IV. DATA INTERPRETATION

As discussed above, the inflexions in the (e,f) curves correspond to structures in the (γ,f) cross section curves [see Eq. (1)]. Thus, we can say that a mere visual inspection of Fig. 3 allows a qualitative delineation of the (γ,f) structures. However, for the delineation of the magnitude of the (γ,f) cross section, we need to perform the unfolding of the (e,f) integrated cross section.

A. Unfolding procedure

We used a least structure unfolding routine developed at our laboratory [4], where the experimental data are fitted with a continuous curve; this curve is input in a subroutine which performs matrix inversion and introduces a smoothing parameter. By varying this parameter, within a previously determined interval, a set of solutions is obtained. Next, each solution is folded back and compared with the experimental data; in this procedure a chi-square is calculated. The accepted solution is the one who provided the closest to unity chi-square. The "smoothing criterion" of the unfolding routine works in such a way that, a structure arising from an isolate statistical fluctuation of two adjacent data points is smoothed out. Thus, only the structure delineated by several consecutive data points, in a wider energy interval, resists to the smoothing.

We performed the unfolding using only $E1$-virtual-photon spectra, calculated in the distorted-wave Born approximation (DWBA) with the inclusion of nuclear size effects [13], because of the following reasons.

Part of the total photoabsorption cross section above the photopion threshold ($\sim$ 140 MeV) corresponds to the quasideuteron absorption mechanism, while another part refers to photopion production. The former consists mostly of $E1$ excitations, and the latter is usually parametrized in $M1$ and $E1$ parts (as described in Refs. [14] and [15]); we represent them by $\sigma_{\rm QD}$, $\sigma_\pi(M1)$, and $\sigma_\pi(E1)$, respectively. Therefore, the general expression for the $e,f)$ cross section is given by

$$\sigma_{e,f}(E_e)=\int_0^{E_e}[\sigma_{\rm QD}(\omega)P_f(E1;\omega)N^{E1}(\omega,E_e)+\sigma_\pi(M1;\omega)P_f(M1;\omega)N^{M1}(\omega,E_e) +\sigma_\pi(E1;\omega)P_f(E1;\omega)N^{E1}(\omega,E_e)]\frac{d\omega}{\omega}. \quad (9)$$

In the electron energy range of our experiment, the shapes and intensities of the $E1$, $M1$, and $E2$ virtual-photon spectra (VPS) become very similar, at least for $\omega > \frac{1}{2}E_e$ [13,16]. We show in Fig. 4 the $E1$ and $M1$ VPS for electrons of 240 MeV scattered by Au, plus the photofission cross section of Au. We note that the (γ,f) cross section below $\sim$ 120 MeV ($\frac{1}{2}E_e$) is nearly two orders of magnitude lower, comparatively to $\omega > 120$ MeV. Therefore, the contribution from $\omega < 120$ MeV to the integrated (e,f) cross section is small; thus, in our approach we can assume that $N^{E1} \cong N^{M1}$, without incurring in errors greater than 3%.

In addition, at excitation energies well above the fission barrier, the nuclear level densities of states populated in $E1$, $E2$, and $M1$ photoexcitation processes have the same magnitude; thus, it is quite reasonable to assume, under statistical grounds, that

$$P_f(E2) \cong P_f(E1) \cong P_f(M1),$$

as pointed out in Ref. [17] (and references therein).

So, Eq. (9) can be rewritten as

$$\sigma_{e,f}(E_e) \cong \int_0^{E_e}[\sigma_{\rm QD}(\omega)+\sigma_\pi(M1;\omega)+\sigma_\pi(E1,\omega)] \times P_f(\omega)N^{E1}(\omega,E_e)\frac{d\omega}{\omega}, \quad (10)$$

where $\sigma_{\rm QD}+\sigma_\pi(M1)+\sigma_\pi(E1)$ is the total photoabsorption cross section $\sigma_{\gamma,a}$ and, as a consequence, the unfolded quantity is $\sigma_{\gamma,a}P_f$ (the photofission cross section $\sigma_{\gamma,f}$).

The fact that $N^{E1} \cong N^{M1} \cong N^{E2}$, at intermediate energies, makes electrofission (and electrodisintegration) cross sections rather insensitive to the relative strengths of the multipoles involved (also discussed in Ref. [18]). Although this renders difficult to obtain information on the multipole composition (which is not the goal of this

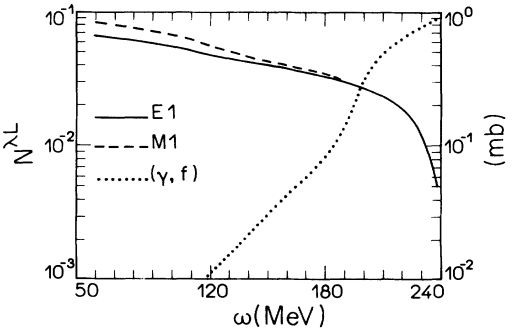

FIG. 4. $E1$ and $M1$ virtual-photon spectra of ^{197}Au, for electrons of 240 MeV, calculated in the DWBA with nuclear size-effects included [13] (left-hand scale), and the unfolded photofission cross section of ^{197}Au (right-hand scale).

work), it does give confidence that the shapes of the unfolded cross sections (based on $E1$ only) are reasonably reliable. Magnitudes are reliable too, as we demonstrated through the comparison of the unfolded (γ, f) cross section of ^{209}Bi with that obtained in Frascati using quasimonochromatic photons (see Fig. 3 of Ref. [4]).

Also shown in Fig. 3 are the unfolded (γ, f) cross sections $\sigma_{\gamma,f}$ of Au and Ta; the uncertainty band of the unfolded curves (not drawn in Fig. 3) is $\sim 15\%$. We note in passing the general feature associated with electro- and photoexcitation yield curves, namely: a structure of, e.g., the (γ, f) curve, around ω', reflects itself as an inflexion of the (e, f) curve around $E'_e = \omega' + \delta$ where, in our energy range, $\delta \approx 10$–20 MeV. This is the so-called "dip effect" of the VPS, which is clearly illustrated by Fig. 3: at $\omega \approx 240$ MeV the VPS intensity is nearly 1 order of magnitude smaller than the intensity at $\omega \approx 220$ MeV.

B. Comparison with previously published results

In Fig. 5 is shown our unfolded (γ, f) cross section of Au, together with those measured at Frascati (with quasimonochromatic photons) and Kharkov (with Bremsstrahlung). Both Fracscati and Kharkov (γ, f) results were generated by deconvolution processes with energy bins equal to 20 MeV, while for our results we used 2 MeV energy bins since a continuous curve was fitted to the experimental (e, f) data points (as explained in Sec. IV A) which, for $E_e \geq 190$ MeV, were measured in steps of 5 MeV. Thus, our data are more sensitive to shape details, while the quasimonochromatic data from Frascati provide better absolute cross-section results.

Except for the (γ, f) dip region between ~ 170 and 200 MeV (see Fig. 5), our results are in excellent agreement with those from Frascati (for $\omega \lesssim 170$ MeV and $\omega \gtrsim 200$ MeV), within the uncertainties. The Bremsstrahlung results from Kharkov, on the other hand, are in agreement only for $\omega \lesssim 170$ MeV.

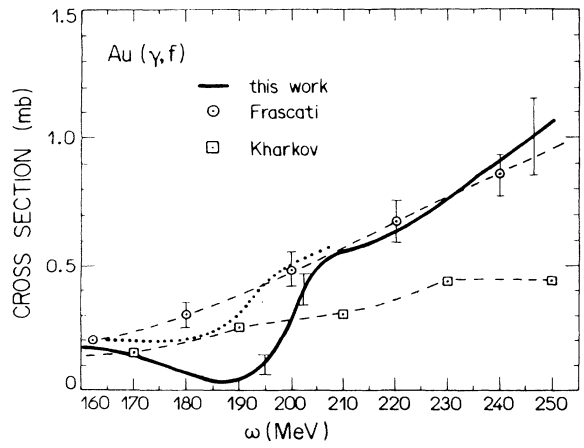

FIG. 5. Photofission cross section of Au: this work (solid curve with uncertainty bars), Frascati (⊙) and Kharkov (⊡). The dotted curve is an alternative unfolding procedure of the photofission yield measured at Frascati (see text). The results from Kharkov were quoted from Ref. [6].

We note that the integral photofission yield measured at Frascati exhibits an inflexion around 190 MeV (see Fig. 1—inflexion with label 2). We decided to play with this inflexion by drawing a smooth curve through the data points around 190 MeV and, next, by performing an unfolding with 2 MeV energy bins. The result of this numerical exercise is shown in Fig. 5 (dotted line)—now we have a (γ, f) dip around 180–185 MeV. At least qualitatively, therefore, our results for Au agree with those from Frascati in the dip region, too. It remains, however, the quantitative disagreement between 170 and 200 MeV. In our favor we can say that we have established a systematics; besides the results for Au and Ta, discussed in this work, we observed similar structures in ^{208}Pb and ^{209}Bi [4,5]. In addition, we are currently measuring the electrofission cross section of ^{182}W; the preliminary results show that the (e, f) yield curve of ^{182}W is remarkably similar to those of Au and Ta.

C. Thermalization related effect

It is quite evident the occurrence of a (γ, f) shoulder at 200–220 MeV (Fig. 3), which cannot be explained in terms of discontinuities neither in $\sigma_{\gamma,a}$ nor in P_f. As discussed in Sec. II, possible strucures in $\sigma_{\gamma,f}$ could be explained only by some sort of distortion in the E_x distribution function $N(E_x, \omega)$, which changes the slope of the "mean-weighted P_f" $\langle P_f \rangle$ [see Eqs. (7) and (8)].

In this regard we note that for $\omega \lesssim 180$ MeV the E_x distribution is practically symmetric around the average value $\bar{E}_x = \frac{1}{2}\omega$, while for $\omega > 200$ MeV $N(E_x, \omega)$ becomes very wide, close to a Maxwell distribution, with a maximum around $E_x = 20$–40 MeV (Fig. 2, and Refs. [7] and [8]). However, at photon energies around 200 MeV we observe a splitting in the E_x-distributions into two well separate structures at $E_x \approx 25$ and 105 MeV. Without going over to any detailed calculations, we observe that the presence of a "high-energy component" in the $N(E_x, \omega)$, at $E_x \approx 105$ MeV, where P_f is much higher relatively to $E_x \approx 25$ MeV, gives rise to a quite enhanced $\langle P_f \rangle$. Since at $\omega \gtrsim 220$ MeV the E_x distributions assume low-energy peaked Maxwellian shapes, it becomes clear that a change in the slope of $\sigma_{\gamma,f}(\omega)$ takes place at $\omega \approx 200$–220 MeV, as experimentally observed.

Besides this qualitative verification, we calculated the (γ, f) cross section for Au using the expression deduced in this work [Eq. (7)], plus the E_x distributions calculated elsewhere [7,8], at photon energies from 180 to 260 MeV; also, we took published values for $\sigma_{\gamma,a}(\omega)$ [19]. The fission probability of the mean compound nucleus (see Sec. II) was calculated by means of well-known statistical based relations [11,17] and procedures [17], plus the assumption that the level density is described by the so-called Fermi gas expression [11]. Since at $E_x \geq 30$ MeV shell effects in nuclei are absent [20], we used liquid-drop quantities calculated by the method of Myers and Swiatecki [21], in order to obtain fission barriers and neutron binding energies for all nuclei participating in the fission-chain decay (see Ref. [7] for more details). The result is shown in Fig. 3; the reproduction of the (γ, f) shoulder,

at 200–220 MeV, is striking within the 15% uncertainty band of the (γ, f) unfolded curve, and particularly if we consider the fact that our calculations have no free adjustable parameter.

As a check of the sensitiveness of the E_x distributions in the delineation of the (γ, f) shoulder, we repeated the calculation of $\sigma_{\gamma,f}(\omega)$ at $\omega = 200$ MeV using a function $N(E_x, \omega)$ with a Maxwellian shape, similar to that at $\omega \gtrsim 220$ MeV; in other words, we simply removed the high-energy component (at $E_x \approx 105$ MeV) of $N(E_x, \omega = 200$ MeV), but we kept the same area under this function. Now, the new $\sigma_{\gamma,f}$ is lowered by a factor of two eliminating, therefore, the shoulder (see the dotted curve in Fig. 3).

It is worth remembering that the function $N(E_x, \omega)$ is determined by the preequilibrium emissions of the thermalization process, that is, the magnitude and the shape of the E_x distribution of the compound nucleus, depend on the *number* and *energy* of the particles (mostly protons and neutrons) emitted in the preequilibrium stage. This stage, by its turn, is governed by the intranuclear cascade process. Therefore, $N(E_x, \omega)$ contains the peculiarities of the nuclear thermalization process. Since the very existence of the (γ, f) shoulder is dictated by both the overall E_x distribution and their fine details (e.g., the "splitting"), as shown by our calculations, we conclude that we have been recognized, for the first time, a thermalization related effect in the fission of Au and Ta. Similar structures previously observed in ^{209}Bi and ^{208}Pb [4,5] are certainly associated to this same effect.

D. Thermalization versus photoexcitation

Although photopion production is the competing photoexcitation mechanism with quasideuteron for $\omega > 140$ MeV, its effectiveness in heating up the nucleus starts at $\omega \gtrsim 200$ MeV. In fact, below this energy pions are photoproduced with kinetic energies $T_\pi < 60$ MeV; in this energy range, the pion mean free path in the nuclear matter is $\lambda_\pi \gtrsim 7$ fm [22] (of the order of the nuclear radius) and, therefore, has a high probability of escaping from the nucleus—as a consequence, small energies are deposited. Thus, quasideuteron absorption is the leading mechanism to excite the nucleus for $\omega \lesssim 200$ MeV.

Up to $\omega \approx 160$–180 MeV the E_x distributions are practically symmetric around $E_x \simeq \frac{1}{2}\omega$; as discussed above, this is the energy region where quasideuteron photoexcitation dominates.

For $\omega \gtrsim 220$ MeV, the photoproduced pions have $T_\pi \gtrsim 80$ MeV, corresponding to $\lambda_\pi \lesssim 2$ fm [22], and are reabsorbed by a pair of nucleons, sharing their rest and kinetic energies. The two interacting nucleons acquire an energy of approximately $\frac{1}{2}\omega$ each (since $\omega \cong T_\pi + m_\pi$, neglecting recoil); before leaving the nucleus these two nucleons loose a small fraction of their energy in inelastic scattering with other nucleons. This is quite understandable since for nucleons with energies $\gtrsim 100$ MeV their mean free paths inside a nucleus are $\gtrsim 6$–7 fm [23] (of the order of the nuclear radius). Thus, from the initial photon energy only a small fraction is converted into excitation energy explaining, therefore, the low-energy maximum in the $N(E_x, \omega)$ functions at $E_x \simeq 20$–40 MeV, which is the common feature at $\omega > 200$ MeV. The broad shape of these distribution functions indicates the occurrence of dispersion effects among the cascade nucleons and the rescattered photopions (before reabsorption).

Under the scenario pictured above, it becomes clear why the E_x distributions around $\omega = 200$ MeV exhibit two maxima. At this energy region there is a change in the nuclear excitation regime, from the dominance of the quasideuteron to that of photopion production. As some sort of "transition region," characteristics of both processes coexist: the peak at $E_x \approx \frac{1}{2}\omega$, due to the quasideuteron process, and the low-energy peak attributed to the onset of the photopion production (as an effective mechanism for the heating up of the nucleus).

Therefore, the competition between the photoexcitation mechanisms determines the peculiarities of the thermalization process which, by its turn, reveals itself in the energy dependence of the photofission cross section, as demonstrated in the present work.

E. Possible fission related structures

Our calculations of $\sigma_{\gamma,f}$, which explain the (γ, f) shoulders experimentally observed for Au and Ta, rely on the assumption that these nuclei decay statistically by fission; this gives rise to fission probabilities strongly increasing with E_x. We would like to discuss the correctness of this assumption.

The fission probability would decrease for an increasing E_x, if substantially less fissionable residual systems are formed; in such a circumstance, a fission related structure could appear in the (γ, f) cross section. In fact, the so-called "saturation effects" in the fission probability are likely to manifest above $E_x = 100$–200 MeV, where preequilibrium emission of heavy fragments (the nuclear fragmentation), and/or the fast nucleon cascade, leads to residual systems that are too light, and/or too cold, to fission (we refer the reader to Ref. [24] for a very detailed discussion on this issue).

However, in the photon energy range of the present work ($\omega \leq 250$ MeV), the mean excitation energies are $\lesssim 85$ MeV [7,8]. Therefore, a significant slowing down of the fission process, comparatively to expectations based on the statistical model, is unlikely.

V. CONCLUDING REMARKS

(1) The result from this work for Au and Ta, plus those previously obtained for ^{209}Bi and ^{208}Pb [4,6], constitute a considerable body of evidences supporting the physical nature of the (e, f) inflexions around 200–220 MeV.

(2) The corresponding (γ, f) structures (or shoulders), associated to these (e, f) inflexions, are nicely described as a direct consequence of fine thermalization related effects around $\omega = 200$ MeV, which dictate the shape char-

acteristics of the E_x-distribution functions $N(E_x, \omega)$.

(3) It is shown that the peculiar shape of $N(E_x, \omega)$ at $\omega = 200$ MeV (double-peaked distribution) is due to an interplay between the two leading photoexcitation mechanisms: quasideuteron and pion photoproduction. In this regard, the role played by the photopion mean free path inside the nucleus is addressed.

(4) Finally, an original formalism for the analysis of photofission at intermediate energies is worked out.

ACKNOWLEDGMENTS

We would like to thank Dr. V. Lucherini and Dr. E. De Sanctis, for providing us with their complete set of results for E_x distributions. Thanks are also due to the Linac crew for providing the specified electron beam. This work was partially supported by Conselho Nacional de Desenvolvimento Científico e Tecnológico (Brazil) and Japan Society for the Promotion of Science.

[1] V. E. Bunakov, Part. Nucl. **11**, 1285 (1980).
[2] A. S. Iljinov, M. V. Mebel, C. Guaraldo, V. Lucherini, E. De Sanctis, N. Bianchi, P. Levi Sandri, V. Muccifora, E. Polli, A. R. Reolon, P. Rossi, and S. Lo Nigro, Phys. Rev. C **39**, 1420 (1989).
[3] V. E. Viola, Nucl. Phys. **A502**, 531c (1989).
[4] J. D. T. Arruda-Neto, M. Sugawara, T. Tamae, O. Sasaki, H. Ogino, H. Miyase, and K. Abe, Phys. Rev. C **34**, 935 (1986).
[5] J. D. T. Arruda-Neto, M. Sugawara, H. Miyase, T. Kobayashi, T. Tamae, K. Abe, M. Nomura, H. Matsuyama, H. Kawahara, K. Namai, M. L. Yonema, and S. Siminonatto, Phys. Rev. C **41**, 354 (1990).
[6] V. Lucherini, C. Guaraldo, E. De Sanctis, P. Levi Sandri, E. Polli, A. R. Reolon, A. S. Iljinov, S. Lo Nigro, S. Aiello, V. Bellini, V. Emma, C. Milone, G. S. Pappalardo, and M. V. Mebel, Phys. Rev. C **39**, 911 (1989).
[7] C. Guaraldo, V. Lucherini, E. De Sanctis, A. S. Iljinov, M. V. Mebel, and S. Lo Nigro, Il. Nuovo Cimento **103A**, 607 (1990).
[8] V. Lucherini (private communication).
[9] K. Kikuchi and M. Kawai, *Nuclear Matter and Nuclear Reactions* (North-Holland, Amsterdam, 1968), p. 244.
[10] J. D. T. Arruda-Neto, A. Deppman, N. Bianchi, and E. De Sanctis, Phys. Rev. C (submitted).
[11] R. Vandenbosch and J. R. Huizenga: *Nuclear Fission* (Academic, New York, 1973), pp. 232, 254, and 255.
[12] J. D. T. Arruda-Neto, M. Sugawara, H. Miyase, T. Kobayashi, T. Tamae, K. Abe, M. Nomura, H. Matsuyama, H. Kawahara, K. Namai, M. L. Yoneama, and S. Siminonatto, J. Phys. G **15**, L215 (1989).
[13] F. Zamani-Noor and D. S. Onley, Phys. Rev. C **33**, 1354 (1986).
[14] B. Ziegler, in *Nuclear Physics with Electromagnetic Interactions*, Lecture Notes in Physics Vol. 108, edited by H. Arenhövel and D. Drechsel (Springer, Berlin, 1979) p. 148.
[15] K. P. Schelhaas, J. M. Henneberg, M. Sanzone-Arenhövel, N. Wieloch-Laufenberg, U. Zurmühl, B. Ziegler, M. Schumacher, and F. Wolf, Nucl. Phys. **A489**, 189 (1988).
[16] P. Durgapal and D. S. Onley, Phys. Rev. C **27**, 523 (1983).
[17] H. Dias, J. D. T. Arruda-Neto, B. Carlson, and M. Hussein, Phys. Rev. C **39**, 564 (1989).
[18] G. J. Miller, J. C. McGeorge, I. Anthony, R. O. Owens, and D. Ryckbosch, Nucl. Phys. **A551**, 135 (1993).
[19] A. Leprêtre, P. Carlos, H. Beil, R. Bergére, J. Fagot, A. De Miniac, and A. Veyssière, Nucl. Phys. **A431**, 573 (1984).
[20] E. A. Cherepanov, A. S. Iljinov, and M. V. Mebel, J. Phys. G **9**, 1397 (1983).
[21] W. D. Myers and W. J. Swiatecki, Ark. Fyz. **36**, 343 (1986).
[22] A. M. Bernstein, in *Photopion Nuclear Physics*, edited by P. Stoler (Plenum, New York, 1979), p. 406.
[23] R. D. McKeown, S. J. Sanders, J. P. Schiffer, H. E. Jackson, M. Paul, J. R. Specht, E. J. Stephenson, R. P. Redwine, and R. E. Segel, Phys. Rev. Lett. **44**, 1033 (1980).
[24] Th. Blaich, M. Begemann-Blaich, M. M. Fowler, J. B. Wilhelmy, H. C. Britt, D. J. Fields, L. F. Hansen, M. N. Namboodiri, T. C. Sangster, and Z. Fraenkel, Phys. Rev. C **45**, 689 (1992).